Improved calculation of the $\gamma^*\gamma \to \pi$ process at low Q^2 using LCSR's and renormalization-group summation[*]

Sergey Mikhailov[1],[*],[**], *Alexandr* Pimikov[1],[***], and *N. G.* Stefanis[2],[****]

[1]Bogoliubov Laboratory of Theoretical Physics, JINR, 141980 Dubna, Russia
[2]Institut für Theoretische Physik II, Ruhr-Universität Bochum, D-44780 Bochum, Germany

Abstract. We study two versions of lightcone sum rules to calculate the $\gamma^*\gamma \to \pi^0$ transition form factor (TFF) within QCD. While the standard version is based on fixed-order perturbation theory by means of a power-series expansion in the strong coupling, the new method incorporates radiative corrections by renormalization-group summation and generates an expansion within a generalized fractional analytic perturbation theory involving only analytic couplings. Using this scheme, we determine the relative nonperturbative parameters and the first two Gegenbauer coefficients of the pion distribution amplitude (DA) to obtain TFF predictions in good agreement with the preliminary BESIII data, while the best-fit pion DA satisfies the most recent lattice constraints on the second moment of the pion DA at the three-loop level.

1 Introduction

In this paper we present our recent work on the calculation of the two-photon process $\gamma^*(Q^2)\gamma(q^2 \sim 0) \to \pi^0$ which contains in the form of a convolution the distribution amplitude of the pion [1]—the simplest bound state in QCD. Our analysis uses the method of lightcone sum rules (LCSR)'s [2, 3] in the extended form developed in [4]. This scheme includes the QCD radiative corrections by means of renormalization-group (RG) summation, ultimately amounting to a generalized version of fractional analytic perturbation theory (FAPT), invented in [5, 6] following [7], and reviewed in [8, 9].

We present the key elements of this formalism and apply it to the recently released preliminary data of the BESIII Collaboration [10, 11], which extend the range of measurements of the $\pi-\gamma$ transition form factor (TFF) to very low $Q^2 \ll 1\,\mathrm{GeV}^2$ values with an unprecedented precision. At such momenta the conventional LCSR method, based on fixed-order perturbation theory (FOPT), cannot describe this transition process with sufficient accuracy, though it works very well at high Q^2 [12, 13]. Very recently, the full QCD calculation of the two-loop coefficient function of leading twist to the TFF $\gamma^*\gamma \to \pi^0$ was carried out analytically by two different groups using different methods and obtaining coinciding results [14, 15]. This level of computational accuracy of the NNLO radiative correction is required by the expected precision of forthcoming data of the Belle II experiment. In the higher Q^2 region, the measured

---

values of $Q^2 F(Q^2)$ reported by the Belle Collaboration [16] agree with the theoretical expectations, while the previous *BABAR* results [17] show above $Q^2 \gtrsim 9$ GeV^2 a rapid growth with Q^2. It is expected that Belle II will collect a large data sample with a much higher accuracy to resolve this discrepancy allowing to test the onset of factorization and identify the scale where asymptotic scaling sets in [18] or establish the existence of scaling violations.

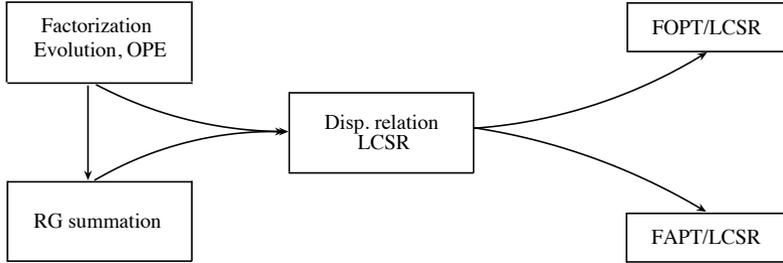The main ingredients of both LCSR methods are shown in Fig. 1.

Figure 1. Schematic derivation of the FOPT and FAPT versions of LCSR's to calculate the TFF.

The paper is organized as follows. In Sec. 2 we present a brief description of the current status of the pion-photon transition form factor (TFF) calculation using LCSR's in FOPT and point out its limitations at $Q^2 \lesssim 1$ GeV^2. In the subsequent section Sec. 3 we discuss the extended version of the LCSR method which incorporates the summation of radiative corrections via the renormalization group. While the first version is sufficient to adequately describe this observable at high-Q^2, see, [13], the second version is more suitable at low momenta, where the radiative corrections, together with the higher twists (twist-four and twist-six) contributions, are particularly important.

2 Radiative corrections in FOPT/LCSR

In this section we briefly address the basic results for the TFF using the method of LCSR's within FOPT in QCD. Applying collinear factorization, the TFF for the hard exclusive process $\gamma^*(Q^2)\gamma(q^2) \to \pi^0$ $(Q^2 \gg q^2 \gg \Lambda^2_{\text{QCD}})$ in leading twist two can be written in convolution form as a power series expansion in the strong coupling $a_s = \alpha_s/4\pi$ to get

$$F^{(\text{tw-2})}_{\text{FOPT}}(Q^2, q^2) = N_{\text{T}} \left(T_{\text{LO}} + a_s T_{\text{NLO}} + a_s^2 T_{\text{NNLO}} + \dots \right) \otimes \varphi_\pi^{(2)}, \tag{1}$$

where $N_{\text{T}} = \sqrt{2} f_\pi/3$. The nonperturbative input of the pion structure is encoded in the lightcone distribution amplitude (DA) of twist two (tw-2), $\varphi_\pi^{(2)}$, which describes the partition of the longitudinal momentum between its two valence quarks with fractions $x_q = x = (k^0 + k^3)/(P^0 + P^3) = k^+/P^+$ and $x_{\bar{q}} = 1 - x \equiv \bar{x}$. The hard coefficient functions are given by the following expressions [1]

$$T_{\text{LO}} = a_s^0(\mu_{\text{F}}^2)T_0(y) \equiv 1/\left(q^2 \bar{y} + Q^2 y\right), \tag{2a}$$

$$a_s T_{\text{NLO}} = a_s^1(\mu_{\text{F}}^2)T_0(y) \otimes \left[\mathcal{T}^{(1)} + \underline{L\ V_0}\right](y, x), \tag{2b}$$

$$a_s^2 T_{\text{NNLO}} = a_s^2(\mu_{\text{F}}^2)T_0(y) \otimes \left[\mathcal{T}_\beta^{(2)} - \underline{L\mathcal{T}^{(1)}\beta_0} + \underline{L\mathcal{T}^{(1)} \otimes V_0} - \underline{(L^2/2)\beta_0 V_0}\right.$$
$$\left. + \underline{(L^2/2)V_0 \otimes V_0} + \underline{LV_1}\right](y, x), \tag{2c}$$

where $L = L(y) = \ln[(q^2\bar{y} + Q^2 y)/\mu_F^2]$ and using the following abbreviations: LO (leading order), NLO (next-to-leading order) and NNLO (next-to-next-to-leading order). Here the terms $\mathcal{T}^{(1)}, \mathcal{T}_\beta^{(2)}$ and $\mathcal{T}^{(2)}$ represent corrections due to parton subprocesses, while the singly and doubly underlined terms are due to $\bar{a}_s(y)$ and Efremov-Radyushkin-Brodsky-Lepage (ERBL) evolution [19, 20] at one loop (V_0 kernel) and two loops (V_1 kernel), respectively. On the other hand, the evolution of the pion DA is taken into account in terms of the conformal expansion

$$\varphi_\pi^{(2)}(z, \mu^2) = \psi_0(x) + \sum_{n=2,4,\ldots}^{\infty} b_n(\mu^2)\psi_n(x), \tag{3}$$

where $\varphi_\pi^{\text{asy}} = \psi_0(x) = 6x(1-x) \equiv 6x\bar{x}$ is the asymptotic pion DA.

3 Radiative corrections using RG summation: FAPT/LCSR

To implement the RG summation in $F^{(\text{tw-2})}$, we collect all underlined evolution terms into the running coupling $a_s(\mu^2) \to \bar{a}_s(y) \equiv \bar{a}_s\left(q^2\bar{y} + Q^2 y\right)$ and the ERBL factor [4] to obtain

$$F_n^{(\text{tw-2})}(Q^2, q^2) = N_{\text{T}} T_0(y) \underset{y}{\otimes} \left\{ \left[\mathbb{1} + \bar{a}_s(y)\mathcal{T}^{(1)}(y, x) + \bar{a}_s^2(y)\mathcal{T}^{(2)}(y, x) + \ldots \right] \right.$$

$$\left. \underset{x}{\otimes} \exp\left[-\int_{a_s}^{\bar{a}_s(y)} \frac{V(\alpha; x, z)}{\beta(\alpha)} d\alpha \right] \right\} \underset{z}{\otimes} \varphi_\pi^{(2)}(z, \mu^2). \tag{4}$$

Employing in Eq. (4) the Gegenbauer expansion given in Eq. (3), we get in leading logarithmic approximation (LLA)

$$F_n^{(\text{tw-2})}(Q^2, q^2) \overset{\text{1-loop}}{\longrightarrow} F_{(1l)n}^{(\text{tw=2})} = N_{\text{T}} T_0(y) \underset{y}{\otimes} \left[\mathbb{1} + \bar{a}_s(y)\mathcal{T}^{(1)}(y, x) \right] \left(\frac{\bar{a}_s(y)}{a_s(\mu^2)} \right)^{\nu_n} \underset{x}{\otimes} \psi_n(x). \tag{5}$$

One realizes that for $q^2 = 0$, $y \ll 1$, the summation of the evolution terms via $\bar{a}_s(y)$ becomes inapplicable, even if Q^2 is large [1].

We now show that this deficit is amended when a dispersion relation for the TFF is involved. The key elements of this procedure can be summarized as follows.

1. Impose factorization and the twist expansion.

2. Use a dispersive form of the TFF

$$\left[F(Q^2, q^2) \right]_{\text{an}} = \int_{m^2}^{\infty} \frac{\rho_F(Q^2, s)}{s + q^2 - i\epsilon} ds, \quad \rho_F(s) = \frac{\text{Im}}{\pi} \left[F(Q^2, -s) \right] \tag{6}$$

   that inevitably leads to FAPT [5, 6] with analytic couplings $\mathcal{A}_\nu$ (Euclidean space) and $\mathfrak{A}_\nu$ (Minkowski space) in a nonpower series expansion.

3. Dissect the spectral density using the perturbative expansion in Eqs. (4), (5), and employing ρ_n for each of the ψ_n harmonics perform the twist expansion:

$$\rho(Q^2, x) = \sum_{0,2,4,\ldots} a_n(Q^2)\rho_n(Q^2, x) + \rho_{\text{tw-4}}(Q^2, x) + \rho_{\text{tw-6}}(Q^2, x) + \ldots, \tag{7}$$

   where the integration variable in the spectral density has been replaced by $s \to x = s/(Q^2 + s)$ and $x_s = s_0/(Q^2 + s_0)$. Then, one obtains the LCSR based on Eq. (6), whereas the FAPT results are encapsulated in the analytic couplings $\mathcal{A}_\nu, \mathfrak{A}_\nu, \mathcal{I}_\nu$. The key point is that the imaginary parts in (6) stem solely from the $a_s^\nu(y)$ factors in Eq. (5). All details of this derivation are discussed in [1].

4. To preserve the perturbative asymptotic limit of the TFF $Q^2 F(Q^2 \to \infty) = \sqrt{2} f_\pi$, the calibration condition $\mathcal{A}_\nu(0) = \mathfrak{A}_\nu(0) = 0$ for $0 < \nu \le 1$ has to be imposed [4]. This yields generalized two-parameter FAPT couplings $\mathcal{I}_\nu$ with explicit expressions given in [1].

Restricting for simplicity our attention to the NNLO_β approximation of the partial form factors F_n within FAPT, we derive in the limits $q^2 \to 0$, $Q(y) \to yQ^2$ the following expression

$$
\begin{aligned}
Q^2 F_{\mathrm{FAPT;n}}^{(\mathrm{tw\text{-}2})}(Q^2) \approx \frac{N_{\mathrm{T}}}{[a_s(\mu^2)]^{\nu_n} [1 + c_1 a_s(\mu^2)]^{\omega_n}} &\left\{ \frac{\mathbb{A}_{\nu_n}(m^2, x)}{x} + \left(\frac{\mathbb{A}_{1+\nu_n}(m^2, y)}{y} \right) \underset{y}{\otimes} \mathcal{T}^{(1)}(y, x) \right. \\
&+ \omega_n c_1 \left[\frac{\mathbb{A}_{1+\nu_n}(m^2, x)}{x} + \frac{\mathbb{A}_{2+\nu_n}(m^2, x)}{x} \frac{c_1(\omega_n - 1)}{2} + \left(\frac{\mathbb{A}_{2+\nu_n}(m^2, y)}{y} \right) \underset{y}{\otimes} \mathcal{T}^{(1)}(y, x) \right] \\
&+ \left. \underline{\underline{\left(\frac{\mathbb{A}_{2+\nu_n}(m^2, y)}{y} \right) \underset{y}{\otimes} \mathcal{T}^{(2)}(y, x)}} \right\} \underset{x}{\otimes} \psi_n(x) ,
\end{aligned}
\tag{8}
$$

where the terms contributing to the TFF in LLA are underlined. The couplings $a_s^\nu(\mu^2)$ and

$$
\mathbb{A}_\nu(m^2, y) = \theta(y \ge y_m) \left[\mathcal{A}_\nu(Q(y)) - \mathfrak{A}_\nu(0) \right] + \theta(y < y_m) \left[\mathcal{I}_\nu(m(y), Q(y)) - \mathfrak{A}_\nu(m(y)) \right]
$$

have to be evaluated with a two-loop running, while $c_1 = \beta_1/\beta_0$ and $\omega_n = [\gamma_1(n)\beta_0 - \gamma_0(n)\beta_1]/[2\beta_0\beta_1]$. The only surviving term in the next-to-leading logarithmic approximation (NLLA) for the numerically important case of the zero-harmonic ($\omega_{n=0} = 0$) is the doubly underlined term. For this reason, the effect of the two-loop evolution in the second line is neglected, i.e., $c_1 = 0$ (for further details, see [1]).

4 FAPT/LCSR for the twist-4 pion TFF

In the previous section we included the RG summation only in the twist-two part of the TFF. To carry out a comprehensive analysis of the experimental data in the low-Q^2 regime $0.35 \le Q^2 \le 3.1 \text{ GeV}^2$, covered by the CELLO [21], CLEO [22], and the preliminary BESIII [10, 11] data, we have to extend the RG procedure to the twist-four term stemming from the contribution of the two-particle DA. To this end, we make the assumption that the three-particle DA term is modified after the RG summation in the same way as the twist-two part and evaluate the complete twist-four contribution in an analogous way.

Following [3], we recast the TFF in the following form

$$
F_{\mathrm{FAPT}}^{\gamma\pi,\mathrm{tw\text{-}4}}(Q^2) = \frac{\sqrt{2} f_\pi}{3Q^2} \left[H_{\mathrm{FAPT}}^{\mathrm{tw\text{-}4}}(Q^2) + \frac{Q^2}{m_\rho^2} k(M^2) V_{\mathrm{FAPT}}^{\mathrm{tw\text{-}4}}(Q^2, M^2) \right],
\tag{9}
$$

$$
V_{\mathrm{FAPT}}^{\mathrm{tw\text{-}4}}(Q^2) = -\frac{\delta_{\mathrm{tw\text{-}4}}^2(\mu_0^2)}{M^2} \int_{\bar{x}_s}^1 dx \, \frac{\Delta_\nu(s_0, \bar{x})}{(a_s(\mu_0^2))^\nu} \frac{\varphi^{(4)}(\bar{x})}{x^2} \exp\left(\frac{m_\rho^2 - Q^2 \bar{x}/x}{M^2} \right),
\tag{10}
$$

$$
H_{\mathrm{FAPT}}^{\mathrm{tw\text{-}4}}(Q^2) = -\frac{\delta_{\mathrm{tw\text{-}4}}^2(\mu_0^2)}{(a_s(\mu_0^2))^\nu} Q^2 \mathbb{A}_\nu(s_0; u) \underset{u}{\otimes} \frac{\varphi^{(4)}(u)}{Q^2(u)},
\tag{11}
$$

where we use the same notations and definitions as in [1]. The expression for the function $\varphi^{(4)}(x)$ below has two terms: the first term in the parenthesis is the two-particle DA contribution while the second term is due to the three-particle DA:

$$
\varphi^{(4)}(x) = \left(\frac{50}{3} + 10 \right) x^2 (1 - x)^2 .
\tag{12}
$$

Note that the part coming from the three-particle DA is included here only heuristically. Due to the RG summation, the three-particle contribution to twist-four should be considered more rigorously, but this lies beyond the scope of this work. For completion, we also quote the value of the twist-four coupling parameter δ^2 together with its FOPT evolution,

$$\delta^2_{\text{tw-4}}(\mu_0^2) = 0.95\, \lambda_q^2/2 = 0.19\ \text{GeV}^2\,,$$

$$\delta^2_{\text{tw-4}}(Q^2) = \left[\frac{a_s(Q^2)}{a_s(\mu_0^2)}\right]^{\nu} \delta^2_{\text{tw-4}}(\mu_0^2)\,, \nu = \gamma_{T4}/\beta_0\,, \gamma_{T4} = 32/9\ [23]\,. \tag{13}$$

The results for $F^{\gamma\pi,\text{tw-4}}\left(Q^2\right)$ in FAPT compared to FOPT are displayed in Fig. 2.
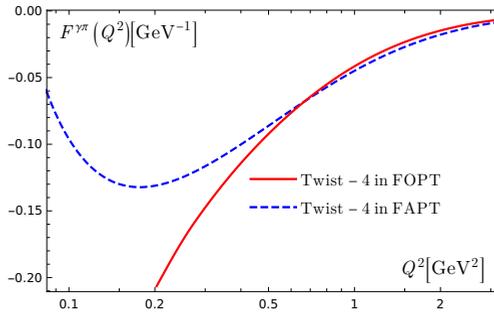

Figure 2. Comparison of the twist-four contribution obtained with FOPT/LCSR's (red solid line) and FAPT/LCSR's (blue dashed line) using in Eq. (9) the single delta-function resonance model with $k(M^2) = 1$.

One may conclude that the FAPT modification of the twist-four contribution provides protection against drastic changes relative to the FOPT behavior, extending this way the applicability domain of the FAPT TFF calculation to lower Q^2 values. On the other hand, both curves come close to each other at $Q^2 > 0.35\ \text{GeV}^2$ so that the estimated ratio (twist-4)/(twist-2) becomes approximately $1/3$ near the lowest BESIII data point, see [10, 11] and Table I in [1].

5 Phenomenological analysis

In this section we present the pivotal phenomenological results of our analysis based on FAPT/LCSR's. This is done for simplicity in terms of $F^{\gamma\pi}_{\text{LCSR}}(Q^2)$ for the harmonics ψ_n, $F^{\gamma\pi}_{\text{LCSR;n}}$, and predictions are shown in Fig. 3 for some selected pion DA's including the best-fit one determined in [1]. Various data from different experiments in the momentum range $0.35 \leq Q^2 \leq 10\ \text{GeV}^2$ are also shown to effect the quality of the fitting procedure at low Q^2.

To this end, we determine the following nonperturbative parameters:

1. b_2, b_4 (conformal coefficients of the twist-2 pion DA) using the following constraints at the scale $\mu_0^2 = 1\ \text{GeV}^2$: $b_2(\mu_0^2) = [0.146, 0.272]$, $b_4(\mu_0^2) = [-0.23, -0.049]$ (domain of twist-2 BMS DA's) [23, 24].

2. $\delta^2_{\text{tw-4}}(\mu_0^2) = 0.19 \pm 0.04\ \text{GeV}^2$ (twist-4 coupling parameter) [23].

3. $\delta^2_{\text{tw-6}}(\mu_0^2) = (1.61 \pm 0.26) \times 10^{-4}\ \text{GeV}^6$ (twist-6 coupling parameter) extracted from the data in [1].

A best fit to the 1σ and 2σ error ellipses of the data up to 3.1 GeV^2 is given in [1] with $\chi^2_{\text{ndf}} = 0.38$. It provides agreement with the N^{3}LO lattice constraints from [25] and yields $b_2(\mu_0^2) = 0.159$, which corresponds to $b_4(\mu_0^2) = -0.098$ if depicted within the BMS domain. Note that the platykurtic (pk) range of pion DA's [26, 27] lies entirely within the 1σ error ellipse of this data set and is close to the NNLO lattice strip [25].
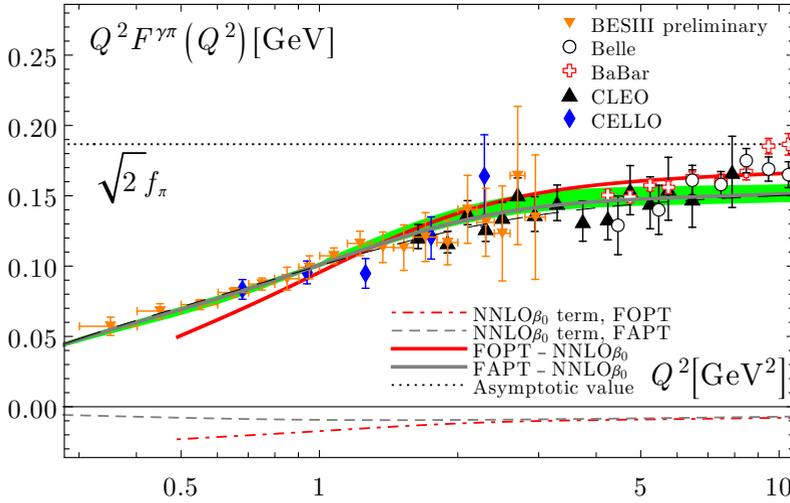

Figure 3. This figure serves to demonstrate that the TFF calculated with FAPT/LCSR's (using $N_f = 3$) compares well with the data up to momenta where it is expected to enter the scaling regime predicted by perturbative QCD, though with reduced accuracy compared to the FOPT/LCSR result, see [13]. The displayed curves are explained in the text.

The TFF predictions calculated this way, are given by

$$F_{\text{LCSR}}^{\gamma\pi}\left(Q^2\right) = F_{\text{LCSR};0}^{\gamma\pi}\left(Q^2\right) + \sum_{n=2,4} b_n(\mu^2) F_{\text{LCSR};n}^{\gamma\pi}\left(Q^2\right) + \delta_{\text{tw-4}}^2(\mu^2) F_{\text{tw-4}}^{\gamma\pi}\left(Q^2\right) + \delta_{\text{tw-6}}^2(\mu^2) F_{\text{tw-6}}^{\gamma\pi}\left(Q^2\right)$$

$$(14)$$

and are displayed in Fig. 3 for the scaled TFF in comparison with various data.

The green strip shows the theoretical uncertainties related to the BMS DAs calculated with QCD sum rules with nonlocal condensates [24]. The induced uncertainty in the low-Q^2 tail is comparable with the errors of the BESIII experiment, while at higher momenta it is smaller than the data errors. The best-fit results, obtained with the pion DA determined in [1], are denoted by the grey solid line (FAPT/LCSR) and the red solid line (FOPT/LCSR in NNLO), respectively. One notices that the analogous prediction obtained with the platykurtic pion DA [26] within FAPT/LCSR (black dashed line) coincides with the outcome based on the best-fit at the level of $\chi^2_{\text{ndf}} = 0.57$. This is significant because this DA amalgamates the key features of NLC's parameterized by the vacuum quark virtuality $\lambda_q^2 = 0.45$ GeV^2 (entailing endpoint suppression) with unimodality—in contrast to the bimodal DA's in the BMS domain with $\lambda_q^2 = 0.40$ GeV^2. We remind that unimodality is welcome because this is a prominent characteristic of pion DA's induced by dynamical chiral symmetry breaking and the emergent generation of hadron mass, see for a recent review [28]. However, such DA's have enhanced tails and fail to reproduce the data with a good accuracy [13].

Finally we note that the dashed curves at the bottom of Fig. 3 representing the dominating contribution NNLO$_\beta$ in FOPT (dashed-dotted line) and FAPT (dashed line) yield above

$Q^2 > 2$ GeV^2 comparable results. This makes it apparent that below $Q^2 \lesssim 1$ GeV^2, the RG summation of the radiative corrections prevents the overestimation of the NNLO contribution in the FOPT/LCSR scheme. A detailed comparison with the total NNLO contribution [14, 15] within our scheme would be useful.

6 Conclusions

In this work we have given a brief presentation of our recent detailed analysis in [1] dealing with the extension of the method of LCSR's provided by the implementation of RG summation of QCD radiative corrections to the $\gamma^*\gamma \to \pi^0$ TFF. We showed that this new scheme inevitably leads to a different perturbative expansion. Instead of a power series expansion in terms of the strong coupling, as in FOPT, on which the standard LCSR method is based, the new perturbation theory employs only analytic couplings amounting to an improved version of FAPT [4]. We used the new FAPT/LCSR scheme [1] to calculate the $F^{\gamma\pi}(Q^2)$ TFF and determined the employed nonperturbative parameters $b_2, b_4, \delta^2_{\text{tw-4}}, \delta^2_{\text{tw-6}}$. To this end, we employed the new preliminary BESIII data [10, 11] in combination with the most advanced lattice calculation of the second moment of the pion DA in three loops [25] and found a bimodal DA which provides a good compromise for all these constraints. The obtained TFF predictions presented above agree with reasonable accuracy also with other data up to $Q^2 = 5$ GeV^2 and beyond with an accuracy that supersedes that of calculations within FOPT at $Q^2 < 1$ GeV^2. Remarkably, the TFF predictions in the FAPT/LCSR scheme obtained with the new best-fit pion DA (Fig. 3) almost coincide with those calculated with the platykurtic pion DA [26], while at the same time both of them are within the uncertainty range (shaded green strip) determined by QCD sum rules with nonlocal condensates [24]. This is important because this DA has a unimodal profile that finds support by the findings of other investigations [28–30] which, however, cannot reproduce the Belle data [16] with the same high accuracy because in contrast to the pk DA, the derived pion DAs are endpoint enhanced [13]. The expected high-precision measurements by the Belle-II Collaboration may provide adjudicative constraints to select the most appropriate pion DA.

Acknowledgments

References

[1] S.V. Mikhailov, A.V. Pimikov, N.G. Stefanis, Phys. Rev. D **103**, 096003 (2021), `2101.12661`

[2] I.I. Balitsky, V.M. Braun, A.V. Kolesnichenko, Nucl. Phys. **B312**, 509 (1989)

[3] A. Khodjamirian, Eur. Phys. J. **C6**, 477 (1999), `hep-ph/9712451`

[4] C. Ayala, S.V. Mikhailov, N.G. Stefanis, Phys. Rev. D **98**, 096017 (2018), [Erratum: Phys. Rev. D 101, 059901 (2020)], `1806.07790`

[5] A.P. Bakulev, S.V. Mikhailov, N.G. Stefanis, Phys. Rev. **D72**, 074014 (2005), [Erratum: Phys. Rev. D72, 119908 (2005)], `hep-ph/0506311`

[6] A.P. Bakulev, S.V. Mikhailov, N.G. Stefanis, Phys. Rev. **D75**, 056005 (2007), [Erratum: Phys. Rev. D77, 079901 (2008)], `hep-ph/0607040`

[7] A.I. Karanikas, N.G. Stefanis, Phys. Lett. **B504**, 225 (2001), [Erratum: Phys. Lett. B636, no.6, 330 (2006)], `hep-ph/0101031`

[8] A.P. Bakulev, Phys. Part. Nucl. **40**, 715 (2009), `0805.0829`

[9] N.G. Stefanis, Phys. Part. Nucl. **44**, 494 (2013), `0902.4805`

[10] C.F. Redmer (BESIII), *Measurement of meson transition form factors at BESIII*, in *13th Conference on the Intersections of Particle and Nuclear Physics (CIPANP 2018) Palm Springs, California, USA, May 29-June 3, 2018* (2018), `1810.00654`

[11] M. Ablikim et al., Chin. Phys. C **44**, 040001 (2020), `1912.05983`

[12] S.V. Mikhailov, A.V. Pimikov, N.G. Stefanis, Phys. Rev. **D93**, 114018 (2016), `1604.06391`

[13] N.G. Stefanis, Phys. Rev. D **102**, 034022 (2020), `2006.10576`

[14] J. Gao, T. Huber, Y. Ji, Y.M. Wang (2021), `2106.01390`

[15] V.M. Braun, A.N. Manashov, S. Moch, J. Schoenleber (2021), `2106.01437`

[16] S. Uehara et al. (Belle), Phys. Rev. **D86**, 092007 (2012), `1205.3249`

[17] B. Aubert et al. (BaBar), Phys. Rev. **D80**, 052002 (2009), `0905.4778`

[18] N.G. Stefanis, *Pion-photon transition form factor in QCD. Theoretical predictions and topology-based data analysis* (2019), `1904.02631`

[19] A.V. Efremov, A.V. Radyushkin, Theor. Math. Phys. **42**, 97 (1980)

[20] G.P. Lepage, S.J. Brodsky, Phys. Rev. **D22**, 2157 (1980)

[21] H.J. Behrend et al. (CELLO), Z. Phys. **C49**, 401 (1991)

[22] J. Gronberg et al. (CLEO), Phys. Rev. **D57**, 33 (1998), `hep-ex/9707031`

[23] A.P. Bakulev, S.V. Mikhailov, N.G. Stefanis, Phys. Rev. **D67**, 074012 (2003), `hep-ph/0212250`

[24] A.P. Bakulev, S.V. Mikhailov, N.G. Stefanis, Phys. Lett. **B508**, 279 (2001), [Erratum: Phys. Lett. B590, 309 (2004)], `hep-ph/0103119`

[25] G.S. Bali, V.M. Braun, S. Bürger, M. Göckeler, M. Gruber, F. Hutzler, P. Korcyl, A. Schäfer, A. Sternbeck, P. Wein, JHEP **08**, 065 (2019), [Addendum: JHEP 11, 037 (2020)], `1903.08038`

[26] N.G. Stefanis, Phys. Lett. **B738**, 483 (2014), `1405.0959`

[27] N.G. Stefanis, A.V. Pimikov, Nucl. Phys. **A945**, 248 (2016), `1506.01302`

[28] C.D. Roberts, D.G. Richards, T. Horn, L. Chang, Prog. Part. Nucl. Phys. **120**, 103883 (2021), `2102.01765`

[29] J.H. Zhang, J.W. Chen, X. Ji, L. Jin, H.W. Lin, Phys. Rev. **D95**, 094514 (2017), `1702.00008`

[30] X. Ji, Y.S. Liu, Y. Liu, J.H. Zhang, Y. Zhao, Rev. Mod. Phys. **93**, 035005 (2021), `2004.03543`